

Exciton self-trapping in twisted hexagonal boron nitride homostructures

Sébastien Roux,^{1,2} Christophe Arnold,² Etienne Carré,^{1,2} Alexandre Plaud,^{1,2} Lei Ren,³ Eli Janzen,⁴ James H. Edgar,⁴ Camille Maestre,⁵ Bérangère Toury,⁵ Catherine Journet,⁵ Vincent Garnier,⁶ Philippe Steyer,⁶ Takashi Taniguchi,⁷ Kenji Watanabe,⁸ Cédric Robert,³ Xavier Marie,³ Annick Loiseau,¹ and Julien Barjon²

¹ *Université Paris-Saclay, ONERA-CNRS, LEM, 92320 Châtillon, France*

² *Université Paris-Saclay, UVSQ, CNRS, GEMaC, 78000, Versailles, France**

³ *Université de Toulouse, INSA-CNRS-UPS, LPCNO, 135 Av. Rangueil, 31077 Toulouse, France*

⁴ *Tim Taylor Department of Chemical Engineering,
Kansas State University Manhattan, KS 66506, USA*

⁵ *Laboratoire des Multimatériaux et Interfaces, UMR CNRS 5615, Univ Lyon
Université Claude Bernard Lyon 1, F-69622 Villeurbanne, France*

⁶ *Laboratoire MATEIS, UMR CNRS 5510, Univ Lyon, INSA Lyon, F-69621 Villeurbanne, France*

⁷ *Research Center for Materials Nanoarchitectonics,
National Institute for Materials Science, 1-1 Namiki, Tsukuba 305-0044, Japan*

⁸ *Research Center for Electronic and Optical Materials,
National Institute for Materials Science, 1-1 Namiki, Tsukuba 305-0044, Japan*

(Dated: 16 mai 2024)

One of the main interests of 2D materials is their ability to be assembled with many degrees of freedom for tuning and manipulating excitonic properties. There is a need to understand how the structure of the interfaces between atomic layers influences exciton properties. Here we use cathodoluminescence (CL) and time-resolved CL experiments to study how excitons interact with the interface between two twisted hexagonal boron nitride (hBN) crystals with various angles. An efficient capture of free excitons by the interface is demonstrated, which leads to a population of long-lived and interface-localized (2D) excitons. Temperature dependent experiments indicate that for high twist angles, these excitons localized at the interface further undergo a self-trapping. It consists in a distortion of the lattice around the exciton on which the exciton traps itself. Our results suggest that this exciton-interface interaction causes a broad optical emission of highly twisted hBN-hBN structures around 300 nm (4 eV). Exciton self-trapping is finally discussed as a common feature of sp^2 hybridized boron nitride polytypes and nanostructures due to the ionic nature of the B-N bond and their compact excitons.

I - Introduction

The conception of 2D material heterostructures (h2D) benefits from a large number of degrees of freedom in the choice of atomic layers and the way they are stacked, creating structural singularities at the interfaces between the layers [1–4]. Taking advantage of these capabilities allows to control and manipulate the properties of excitons : the efficiency of their radiative recombination [5–10], the properties of their emission [11], their diffusion length and their valley and/or spin coherence [12, 13], the dielectric screening between the electron and the hole [14–17]. Finally, excitons can interact with Moiré-superpotentials, which tune their properties and motion [18–24]. Thus, h2Ds offer an ideal platform for creating novel electronic devices using exciton fluxes (excitronics) [25], or using their spin/valley indices (valleytronics and spintronics) [26]. Hexagonal boron nitride (hBN) is present in most h2D since it is the best insulating material for use as a substrate or as a capping layer for other 2D materials such as transition metal dichalcogenides (TMDs), 2D magnets [27] and graphene [11, 14, 28–32]. Because hBN plays such a key role in h2D-based devices, it is crucial to understand the surface and interface effects associated with it.

The simplest hBN-based h2D is the twisted hBN-hBN homostructure, which consists of two hBN crystals with different in-plane crystal orientations. These structures exhibit many properties that are not present in single hBN crystals. At small twist angles, triangular ferroelectric domains appear at the interface [33, 34], as well as drastic changes in the electronic properties, such as in some cases, a spatial separation of the electron and hole wave functions within the Moiré supercell [35, 36]. At high twist angles, hBN-hBN homostructure exhibits intense second harmonic generation, which could be modulated by the twist angle [37]. Finally, a new luminescence signal has recently been discovered in cathodoluminescence (CL) on twisted hBN-hBN structures. It is characterized by a large linewidth (2 eV) and a maximum intensity at 4 eV (300 nm wavelength), i.e. 2 eV below the hBN gap [38, 39]. The origin of this optical emission and of the 2 eV redshift is debated. First, a giant exciton trapping at the interface Moiré was proposed [39, 40]. However, this is not consistent with theoretical studies, which estimate the depth of the interface energy well to be only a few hundreds of meV for excitons [41, 42]. Therefore, another group has discarded its excitonic nature and rather attributed this emission to deep defects near the interface [41].

An alternative explanation involved the occurrence of exciton self-trapping at the interface of the homostructure. The phenomenon of self-trapping of an electron, hole, or exciton was predicted theoretically in the 1930s [43, 44] and demonstrated experimentally in alkali halide crystals as early as the 1960s [45–49]. Self-trapping results from a local deformation of the crystal lattice around a charged particle (or dipole) where the particle (or dipole) is trapped. The particle (or dipole) induces the lattice deformation, hence the term “self-trapped state”. This state is a kind of polaron : a charge associated with the deformation cloud it induces around itself. If the coupling with the deformation mode is strong enough, the self-trapped state is more energetically stable than the Bloch state of the free particle in the undeformed lattice [43]. hBN is a good candidate for exciton self-trapping since it is a highly ionic material with a very compact exciton [50], which makes excitons and atomic B-N bonds dipoles of similar size, which is expected to favor exciton-lattice interactions.

Today, the puzzle for understanding the nature and the origin of this new optical emission is incomplete. In this work, we present a deterministic approach to elucidate the interplay between twist angles, defects and excitons using continuous and time-resolved cathodoluminescence. To this end, sixteen hBN-hBN structures with different twist angles and fabricated from different hBN crystal sources are studied in cathodoluminescence (CL), in time-resolved CL (TRCL), at room temperature and as a function of temperature. We show how the whole set of experimental data support an exciton self-trapping mechanism occurring at the interface of hBN-hBN homostructures.

II – Experiments

All cathodoluminescence (CL) experiments were performed using a JEOL7001F scanning electron microscope (SEM) equipped with a Horiba Jobin-Yvon CL system optimized for UV detection, as described in detail in reference [51]. Secondary electrons are detected by a Everhart-Thornley detector (SE detector). The SEM image corresponds to the intensity of the signal collected by the SE detector as a function of the position of the focused electron beam, with an ultimate spatial resolution of 1.2 nm. Cathodoluminescence images are measured by a photomultiplier (Hamamatsu HJY model - cooled to -30°C by Peltier effect) as the electron beam scans the selected area of the sample. The signal from the SE detector and the intensity collected by the photomultiplier are recorded simultaneously. In this way, SEM and CL images of the same area are generated, which allows to correlate the emission of a CL signal with the topography of the sample. The CL image can be panchromatic (total intensity, unfiltered) or monochromatic, filtered in

wavelength by monochromator equipped with diffraction gratings. Cathodoluminescence spectra are recorded with a CCD camera.

Thanks to a careful calibration in intensity [51], the internal quantum efficiency (*IQE*) of a luminescence signal can be evaluated from a CL spectrum. It corresponds to the ratio between the rate of photons emitted inside the sample and the rate of electron-hole pairs generated by the incident electron beam. Details of the *IQE* measurement for the considered signal are given in the Appendix A. Finally, time-resolved CL (TRCL) experiments are performed using a custom-built beam-blanking device mounted on the SEM column with a time resolution of 100 ps (details of the setup are presented in ref. [50]).

To study the emission of twisted hBN-hBN structures, we decided to vary a large number of parameters in the fabrication of the homostructures : the twist angle, the thickness of the crystal flakes in stack, but also the quality of the starting hBN crystals and the way the two crystal flakes are assembled. hBN crystals with natural boron isotope content were grown by three different processes : an Atmospheric Pressure High Temperature (APHT) process [52?–54] from Ni/Cr solvent, a High-Pressure High Temperature (HPHT) route [55, 56], and a Polymer Derived Ceramic (PDC) method [57?]. hBN from the HPHT method is recognized in the 2D materials scientific community as the reference hBN crystals. In a previous study, a quantitative benchmarking of the respective quality, in terms of defect density, of these different hBN sources was performed based on the measured free exciton lifetimes [50]. The values of the lifetime and *IQE* of the free exciton measured on bulk crystals from the different hBN sources are given in Tab. I.

To fabricate twisted homostructures made of HPHT crystals, the bottom hBN layer is mechanically exfoliated using a PDMS viscoelastic stamp and then deposited onto a Si/SiO₂ substrate [59]. The second hBN flake is exfoliated in the same manner, aligned under a microscope over the first crystal flake and then deposited on top of it. Finally, the samples are annealed at 150°C for 1h30 on a hot plate. Note that with this method, one atomic layer that composes the twisted interface was in contact with the polymer.

For twisted homostructures made of APHT and PDC crystals, the bottom layer of hBN is mechanically peeled off using Scotch tape on a Si/SiO₂ substrate, according to the method originally developed for graphene [60]. Since the interaction between the tape and the hBN flake is stronger than the Van der Waals interactions between the hBN layers, only part of the crystal can be detached and transferred on the substrate. The lower hBN surface is thus freshly cleaved. The second flake of hBN is peeled off using Scotch tape on PDMS, aligned, and then deposited onto the bottom hBN flake [59]. This method ensures that the two atomic layers that make up the

hBN-hBN interface have never been in contact with either the PDMS or the Scotch tape. The procedures were performed in a controlled atmosphere glove box.

The twist angle between the two hBN flakes is measured in diffraction by electron backscatter diffraction (EBSD) or by backscattered electron channeling pattern (ECP), as shown in Fig. 1 for 3 HPHT samples. Details of the twist angle measurement are presented in the Appendix B. The samples are named according to the crystal synthesis method from which they are issued (HPHT, APHT or PDC) and the twist angle. Tab. I lists the different samples and the respective thickness of the top and bottom parts measured by Atomic Force Microscopy (AFM).

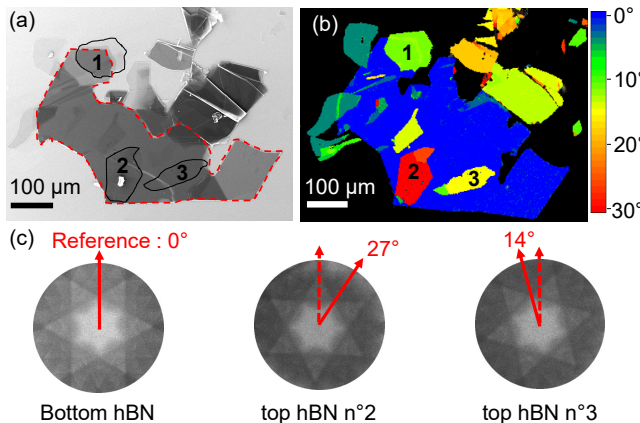


FIGURE 1. (a) SEM image of 3 hBN-hBN homostructures fabricated from an HPHT bulk crystal. The lower hBN flake is indicated by red dotted lines. The upper hBN flakes are numbered from 1 to 3 and surrounded by solid black lines. (b) EBSD mapping of the in-plane crystal orientation of the hBN flakes. The orientation of the bottom hBN crystal is taken as the reference for evaluating the twist angle of the top hBN. (c) ECP recorded on the lower hBN crystal and upper hBN crystals n° 2 and n° 3.

III - Evidence of the excitonic origin of the broad 300 nm optical emission

All hBN-hBN samples were first analyzed using continuous excitation CL (cw-CL) at room temperature. The first observation is that the luminescence at 300 nm mainly appears in homostructures with high twist angles (Fig. 2). At low twist, such as the PDC-2°, APHT-3° and APHT-4° samples, no luminescent signal could be detected in the 250-400 nm range, confirming a recent study [39]. We conclude that luminescence at 300 nm becomes truly significant at angles greater than 5°. A spectrum measured on a low angle hBN-hBN structure is presented in the Appendix C. Spectra obtained on 3 highly twisted hBN-hBN homostructures (purple) and on a single hBN crystals as a reference (black) are shown in Fig. 2(b). The

Sample	215 nm <i>IQE</i> (%) [50]	τ (ns) [50]	Top hBN (nm)	Bottom hBN (nm)
HPHT-11°	18	4.2	260	730
HPHT-14°			15	290
HPHT-15°			17	990
HPHT-23°			9	220
HPHT-27°			13	990
APHT-3°	4.2	0.99	60	40
APHT-4°			67	37
APHT-10°			84	38
APHT-13°			100	60
APHT-29°			20	50
PDC-2°	1.7	0.43	27	46
PDC-13°			68	46
PDC-16°			310	125
PDC-18°			310	370
PDC-19°			44	46
PDC-26°			102	46

TABLE I. Presentation of the 16 hBN-hBN samples of the present study and the respective thickness of top and bottom flakes. The *IQE* and the lifetime (τ) of the free exciton measured on bulk crystals from the same sources [50] are indicated to quantitatively compare the quality of the samples.

broad 300 nm emission is modulated by Fabry-Pérot interferences whose periodicity is consistent with the flakes thickness (see Tab. I). The signals are comparable for all samples, whatever the hBN source and flakes thicknesses. It displays common characteristics to previous observations [39–41] : very broad luminescence ranging from 250 to 400 nm (2 eV width), intense and centered around 300 nm, redshifted by 2 eV compared to the bulk hBN free exciton luminescence at 215 nm.

CL images filtered at 300 nm are presented in Fig. 2(c) and reveal that this emission is only detectable when the two twisted hBN crystals are in contact. These images clearly show that the 300 nm cathodoluminescence is associated with the presence of an interface between the two twisted hBN crystals. In summary of these first observations, the detection of the broad 300 nm optical emission appears independent of the quality of the hBN crystal, which varies greatly depending on the hBN synthesis process [50]. The emission phenomenon is therefore very robust. It appears unconditionally as soon as the twist angle is large, as already reported in Ref. [39] for instance.. As it does not depend on the differences in nature and density of defects that present the three hBN sources used to fabricate the homostructures, the emission seems to be intrinsic to the presence of the interface itself rather than related to extrinsic defects. This raises the question of its origin and more specifically of the interplay between the exciton and the interface of the homostructure, that we will explore in the following using TRCL.

The goal of the TRCL study is to identify the role of bulk free excitons in the process leading to the lumines-

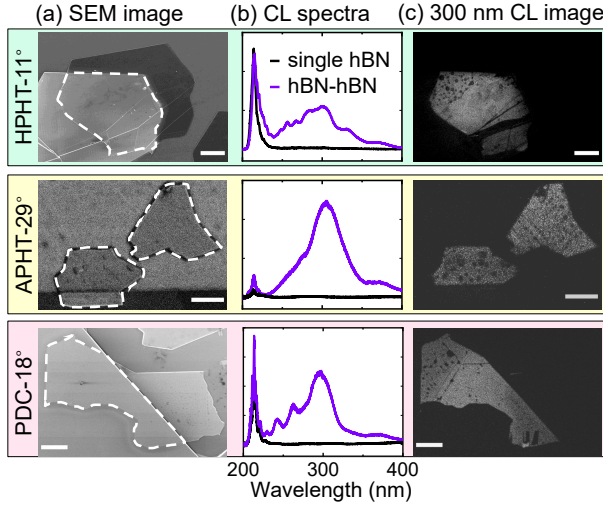


FIGURE 2. (a) SEM images of the twisted homostructures, outlined with a dotted line; (b) CL spectra measured on the bottom crystal alone (in black) and on the homostructure (in purple) at 300 K; (c) CL images filtered at 300 ± 7.5 nm at 300 K, on HPHT-11° (5 kV, 27 pA), APHT-29° (3 kV, 280 pA), and PDC-18° (5 kV, 340 pA) samples. Scale bars are 10 μ m.

cence at 300 nm. It has been performed on HPHT based homostructures at room temperature. Fig. 3(a) compares the decay of the free exciton luminescence at 215 nm in the HPHT-11° homostructure with the decay obtained on the bottom hBN crystal alone. A drastic change is observed. For the crystal alone, the decay is dominated by a short 3 ns component, typical of the TRCL decay of the free exciton in a single bulk HPHT-hBN crystal [50]. For the homostructure, the fast initial component is similar but a long component of 0.46 μ s appears with a significant intensity (30% on the HPHT-11° sample). This long time is much larger than the radiative lifetime of the free exciton measured at 27 ns [50]. This long-lived free exciton dynamics appear only in the presence of a twisted hBN-hBN interface. This could therefore be attributed to a significant detrapping of excitons from the interface. It shows the existence of a reservoir of excitons trapped at the interface and implies their prior trapping. TRCL thus reveals a phenomenon of trapping-detrapping of free excitons at the interface. It results in the coupling of the population of free excitons in the volume of the hBN crystals with the population of long-lived excitons captured at the interface between the twisted crystals.

As shown in the Appendix D, the temporal decay of the broad 300 nm luminescence is independent of wavelength from 250 to 400 nm. This suggests that this large signal does not originate from an ensemble of quantum emitters with different energies.

Fig. 3(b) compares the decay of the free excitons in the hBN bulk crystal at 215 nm and the decay of the 300 nm luminescence both recorded in TRCL on the HPHT-11°

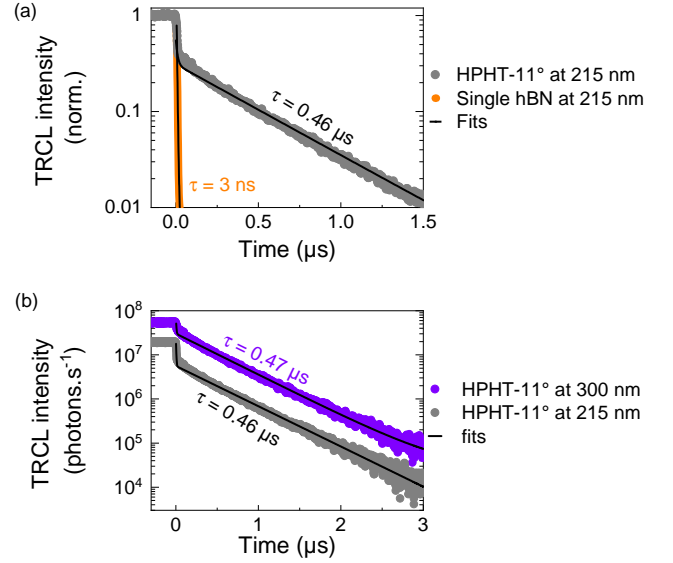


FIGURE 3. (a) Decay of the free exciton luminescence, filtered at 215 ± 7.5 nm, on the bottom hBN alone (gray) and on the hBN-hBN twisted structure HPHT-11° (orange), after interrupting the TRCL excitation at initial time (5 kV, 27 pA, spot size of 10 μ m). Bi-exponential decay functions are used for the fits. (b) Decay of the free exciton luminescence (black), and of the the 300 nm emission (purple), filtered at 300 ± 7.5 nm, after interruption of steady excitation at $t=0$, on HPHT-11° homostructure (5 kV, 27 pA, 10 μ m excitation spot diameter). Intensities during steady state excitation ($t < 0$) are normalized by the integrated intensity of the bands recorded on continuous CL spectra. Experiments done at 300 K.

twisted homostructure. Without going into the quantitative analysis of the characteristic times of the decays (presented later), we already note that the characteristic decay time of the the 300 nm luminescence is equal to the characteristic time of the long component of the free exciton at 215 nm. This means that the 300 nm luminescence is fed by the population of excitons trapped at the interface. The TRCL experiments demonstrate that the 300 nm luminescence originates from the trapping of free excitons at the interface. Still, the radiative process has to be identified, which is the subject of the next parts.

IV - Power dependence and internal quantum efficiency of the 300 nm emission.

During CL experiments, the electron beam excitation is spread in depth, so that the hBN-hBN interface is indirectly excited by the diffusion of free excitons generated in the volume of the hBN crystals towards the interface between them [61]. The efficiency of the interface exciton luminescence at 300 nm is then equal to the efficiency of the transport of free excitons from the volume to the interface times the efficiency of the radiative recombination

process at the interface.

The luminescence from the twisted hBN-hBN homostructures is analyzed here as a function of the areal density of the excitation power (W.cm^{-2}). Low power density data were recorded with an acceleration voltage of 5 kV with a constant current of 27 pA and spot diameters ranging from 1.6 to 26 μm . High power densities were obtained with a fixed spot diameter of 1.6 μm and excitation currents ranging from 27 to 5 600 pA. This dual approach made it possible to vary the excitation power density over 5 orders of magnitude. Fig. 4(a) shows the

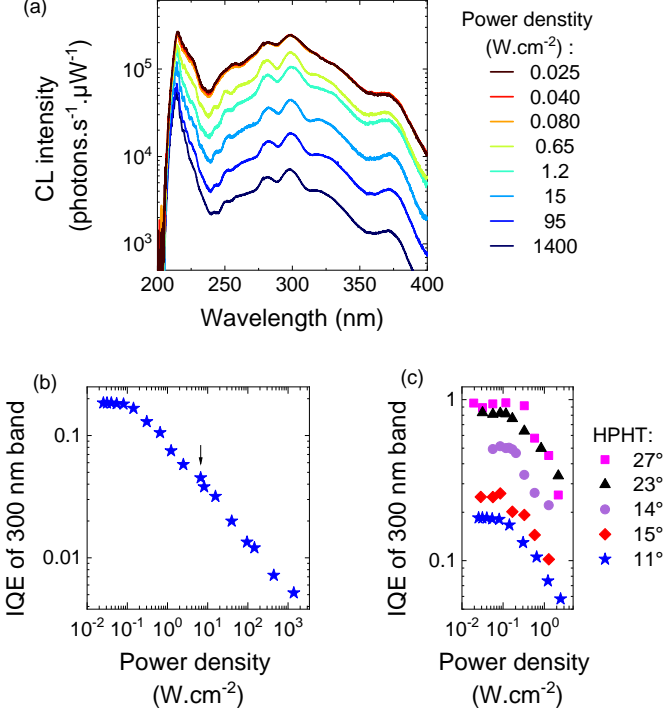


FIGURE 4. (a) CL spectra normalized by the excitation power for different excitation densities (5kV, 300K) measured on the HPHT-11° sample (b) *IQE* of the 300 nm emission, deduced from (a), as a function of the excitation power density. The black arrow indicates the transition point between the two methods for varying the excitation density, as indicated in the text. (c) *IQE* of the 300 nm emission as a function of excitation density for the 5 HPHT samples.

spectra normalized by the excitation power for different excitation densities on the HPHT-11° sample. Fig. 4(b) further shows that the *IQE* of the 300 nm luminescence, measured on the spectra on (a), decreases by a factor of 30 between 0.1 and 1400 W.cm^{-2} . This decrease reveals a non-linearity in the excitation of the 300 nm emission that appears at extremely low power densities. Fig. 4(c) shows that this saturation effect appears systematically above $10^{-1} \text{ W.cm}^{-2}$. Note that the twist angle seems to have a minor effect on the saturation threshold. This plot provides a practical guideline for employing CL excitation conditions that avoid non-linear effects in the sample

study.

More interestingly, for excitation densities below 0.1 W.cm^{-2} , Fig. 4(c) shows that the *IQE* of the 300 nm luminescence from the interface can reach surprisingly high values, close to unity. The *IQE* results are presented in Tab. II. The higher the twist angle, the higher the *IQE* of the 300 nm luminescence. The *IQE* approaching 100% near a 30° twist is a very rare phenomenon at 300 K and may be promising for light emitting devices. This means that (i) the transport of free excitons from the crystal volume to the interface has an efficiency close to 100%, which is not surprising considering the exciton out-of-plane diffusion lengths measured in HPHT samples [61], and (ii) close to 30° twist angle, the mechanism at the origin of the 300 nm luminescence from the interface has an efficiency close to 100%. This means that close to 30°, almost all excitons trapped at the interface recombines with a photon emission within the 300 nm band.

Sample	300 nm <i>IQE</i> (%)
HPHT-11°	20
HPHT-14°	50
HPHT-15°	30
HPHT-23°	80
HPHT-27°	90

TABLE II. *IQE* of the 300 nm emission measured below 0.1 W.cm^{-2} on twisted hBN homostructures made of HPHT crystals.

Note that between 10^{-2} and $10^{-1} \text{ W.cm}^{-2}$, the average energy of the photons emitted within the broad 300 nm band is slightly red-shifted by about 15 meV when increasing the power. In contrast, a donor-acceptor pair (DAP) emission, which would have been a candidate for such a broad luminescence, shows a clear blue shift with increasing power excitation [62, 63]. This provides a strong evidence that the 300 nm emission of hBN-hBN structures is not due to DAP recombinations.

V– Exciton self-trapping at the twisted hBN-hBN interface

The characteristics of the 300 nm emission (2 eV energy shift and the 2 eV broadening) supports a self-trapping mechanism of excitons at the interface that we develop in this section. Fig. 5(a) illustrates the difference between simple exciton trapping in the potential well formed by the interface between the two twisted hBN flakes (X_{2D}) and self-trapping of this exciton at the interface (X_{ST}). A self-trapped exciton is an exciton that induces a lattice distortion around it, and that is trapped in this distorted area. The configuration diagram drawn in Fig. 5(b) displays the exciton energy as a function of the lattice deformation around it, represented by the configuration coordinate. In this diagram, we define the trapping

energy potential of the twisted interface at zero deformation, denoted E_T , which is estimated in the order of 100 meV according to theoretical calculations [41, 42], as well as an energy barrier to the self-trapping, denoted E_{FST} . The possibility of crossing an energy barrier for self-trapping was predicted by Landau [43] and Toyozawa [64] for electrons and by Rashba [65, 66] and Sumi and Toyozawa [67] for excitons. This was demonstrated experimentally in the 60's and 70's for self-trapped excitons on alkali halides [68–70]. The barrier disappears only in the case of self-trapping of an exciton previously trapped on a 0D site [66, 71]. The presence of this energy barrier implies the coexistence of excitons simply trapped at the 2D interface (X_{2D}) and excitons self-trapped at the interface (X_{ST}). By adding the free excitons of the 3D bulk hBN (X_{3D}), there are thus three coupled exciton populations during the CL experiments. Note that the energy barrier for self-trapping is necessarily low, since luminescence of X_{ST} occurs close to liquid helium temperature (see Appendix E). However, it can limit the formation of X_{ST} and reduce the intensity of their luminescence as the temperature is lowered [68–70]. In this process, radiative recombination of a self-trapped exciton is accompanied by the emission of a set of phonons to restore the crystal lattice to its undistorted form as sketched in Fig. 5(b). This drastically reduces the energy of the emitted photon with respect to the band gap of the interface and explains the large energy shift (≈ 2 eV) between the excitonic bandgap and the luminescence at the interface. Furthermore, the curvature of the ground state at high distortion is such that recombining self-trapped excitons inherently leads to very broad emission. This is illustrated in Fig. 5(b), where the three purple arrows (solid lines) represent photons of different energies resulting from the recombination of self-trapped excitons at the band edge.

Experimentally, emission related to excitons trapped at the interface (X_{2D}) has not been detected in CL. Two possible scenarios can be considered to account for the zero-luminescence intensity : 1) the X_{2D} population is zero, 2) the X_{2D} excitons are dark, i.e. have an infinite radiative lifetime. On one hand, in the first scenario, excitons necessarily accumulate at the interface in the X_{ST} state, which, first, requires their self-trapping to be instantaneous, and, second, implies that the detrapping of excitons from the interface into the volume (shown earlier) occurs from the X_{ST} states. This seems to contradict the presence of the energy barrier to self-trapping that we emphasized earlier and that limits the formation of X_{ST} . Furthermore, detrapping from an X_{ST} state to an X_{3D} state requires the emission of a large number of phonons necessary to restore the lattice to its undistorted form, which will be energetically too costly. On the other hand, in the scenario 2, X_{2D} excitons have a negligible probability of radiative recombination (dark excitons). This seems to be consistent with (i) the non-radiative nature

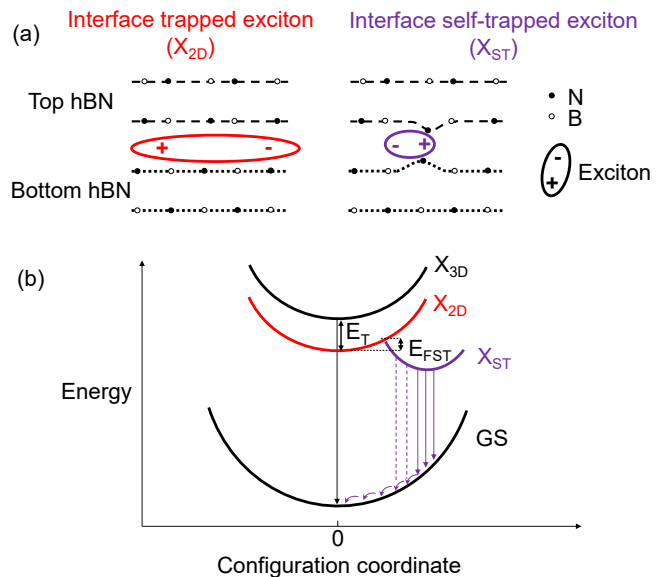


FIGURE 5. (a) Diagram of a trapped exciton at the interface (X_{2D}), in red, and of a self-trapped exciton at the interface (X_{ST}), in purple, with a self-induced lattice deformation on which the exciton is trapped. (b) Configuration coordinate diagram representing the three excitons populations in hBN-hBN structures : X_{3D} , X_{2D} and X_{ST} . The exciton trapping potential of the interface at zero distortion appears as E_T between X_{3D} and X_{2D} . The energy barrier for the formation of the self-trapped exciton is indicated (E_{FST}). The long straight arrows represent the photons resulting from the radiative recombination of free excitons (in black), of thermalized self-trapped excitons (purple, solid lines), and of non-thermalized self-trapped excitons or "hot" self-trapped excitons (purple, dashed line). The small curved arrows represent the phonons required for the lattice to return to the ground state during the recombination of a self-trapped exciton.

of the free surface [61], (ii) the long lifetime of the interface excitons evidenced in Fig. 3, and (iii) the IQE close to 100% observed for X_{ST} at high twist angles (Tab. II), implying that the recombination rate of X_{2D} is very low compared to that of X_{ST} . Therefore, we have ruled out scenario 1 and in the following we will only consider scenario 2. Since the bright recombinations are dominant at high angles (see table II.), we will also neglect the non-radiative recombinations of X_{2D} .

VI - Temperature-dependent investigations.

In order to strengthen the attribution of the 300 nm emission to a self-trapping process, and to characterize the different exciton populations in more details, we have performed a series of experiments as a function of temperature. We first studied the spectral features of the 300 nm luminescence. Fig. 6(a-b) shows the cw-CL spectra recorded on the HPHT-11° sample, at very low power density (5 kV, 27 pA, 60 μ m spot diameter) to avoid

saturation effects. Since saturation could not be avoided below 100 K even at this very low power density ($\approx 0.005 \text{ W.cm}^{-2}$), we limited the measurements to the 100-300 K range.

Non-thermalized (hot) self-trapped excitons are favored at high temperatures, and their recombination, shown in Fig. 6(b), occurs at a higher energy than when they are thermalized to their energy minimum. Theoretically, we therefore expect a slight increase in the emission energy of self-trapped excitons as the temperature increases [72, 73]. Between 200 and 300 K, there is a blue shift of the X_{ST} exciton luminescence in the 250-300 nm range, consistent with a contribution from non-

thermalized X_{ST} that increases at higher temperatures (hot X_{ST} in Fig. 6). This broadens the emission towards high energies, as characterized by the increase in the standard deviation of the emission energy (Fig. 6(c)) and the shift of the average energy of the X_{ST} emission (Fig. 6(d)). Note that the spectral width of the hBN-hBN 300 nm luminescence still remains around 2 eV at cryogenic temperatures, as shown in the Appendix E. This is in complete contrast to the color center emission that can also occur on some hBN-hBN structures and on single hBN flakes, which exhibit very narrow linewidths at 5K [74]. This clearly indicates that the luminescence from the color centers and from the hBN-hBN interfaces are of different natures.

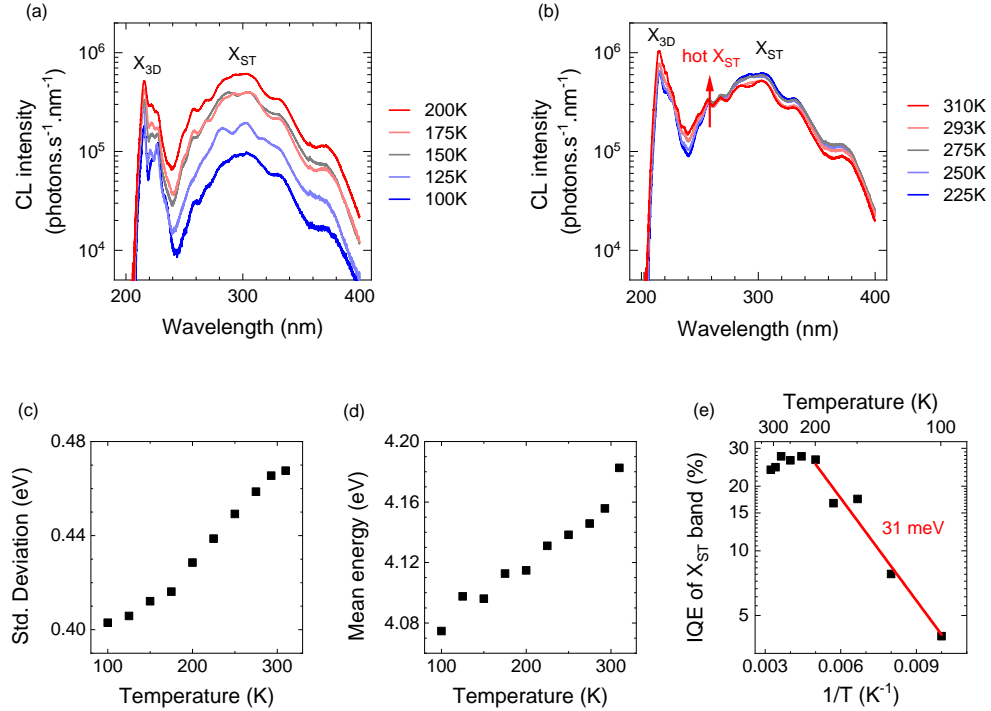


FIGURE 6. (a-b) Spectra recorded on the HPHT-11° sample between 100 and 310 K. (c) Standard deviation of the emission energy, (d) average emission energy, and (e) IQE of the self-trapped exciton X_{ST} luminescence as a function of temperature. An Arrhenius law is shown in red, from which an activation energy of about 30 meV is extracted.

Fig. 6 (e) shows that the IQE of the X_{ST} luminescence drops below 200 K, and is only a few percent at 100 K. The activation of X_{ST} emission with temperature is consistent with an energy barrier for self-trapping (named E_{FST} in Fig. 5(b)). We evaluate this energy E_{FST} with an Arrhenius plot fit. We find an E_{FST} value of 31 meV. This value is undoubtedly overestimated due to saturation, which is probably not completely avoided at about 100 K, and is subject to a high uncertainty due to the small temperature range. It is therefore reasonable to estimate the activation of self-trapping in this sample to be around 10 meV. This is the order of magnitude found in the literature for the self-trapping of excitons in other materials such as alkali halides [68, 70, 72, 75, 76].

The various effects revealed by these first temperature-dependent experiments are all consistent with an emission resulting from the recombination of excitons self-trapped at the twisted hBN-hBN interface.

On this basis, we now explain the recombination dynamics of the three exciton populations in hBN-hBN homostructures (X_{3D} , X_{2D} and X_{ST}), considering the interactions that bind them, in order to ascribe a physical meaning to the decay times in Fig. 3. The characteristic time constants of the different transitions between the different exciton populations are shown in Fig. 7. X_{2D} accumulate with a rate C at the interface following the efficient capture of the free excitons generated by the primary excitation at the interface. They are then slowly

converted, at a detrapping rate D , to X_{3D} or self-trapped in the X_{ST} states at a rate ST . According to this scenario,

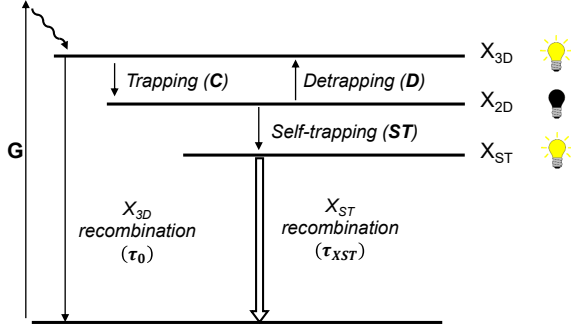


FIGURE 7. Scenario of energy levels and transitions between the three exciton populations within the twisted hBN-hBN homostructures. In this scenario, excitons from volume (X_{3D}) are trapped at the interface, where they accumulate in the dark and long living form (X_{2D}). Once self-trapped (X_{ST}), they recombine very efficiently with a photon emission, leading to the intense emission at 300 nm.

rio, the long decay time of X_{3D} and X_{ST} measured in TRCL (τ_l) after the interruption of the continuous excitation (see Fig. 3) corresponds to the lifetime of the X_{2D} excitons that feed the X_{3D} and X_{ST} populations when they detrapped or self-trapped. Considering the detrapping (rate D) and self-trapping (rate ST) of X_{2D} , τ_l is given by: $1/\tau_l \approx D + ST$ (Details of the calculation are given in the Appendix F.). From this relation, the detrapping rate D can be evaluated from temperature-dependent TRCL measurements of the long decay time of X_{3D} and X_{ST} . These decay times are similar for both exciton populations when decreasing the temperature (see Fig. 3 for room temperature), so we present the measurements only for the free excitons luminescence. The results are shown in Fig. 8(a) for HPHT-11° sample. The decays are normalized by the integrated intensity of the X_{3D} band measured by CL spectroscopy under continuous excitation (spectra in Fig. 6(a-b) for sample HPHT-11°). The characteristic time of the long component τ_l is extracted from bi-exponential function fits. Fig. 8(b) is a plot of $1/\tau_l \approx D + ST$ as a function of $1/T$ (K). The data are fitted with an Arrhenius function from which an activation energy of 110 meV is extracted. Given the low activation energy for the formation of self-trapped excitons (E_{FST}), previously estimated to be around 10 meV, $1/\tau_l \approx D + ST$ appears to be limited by the thermal activation of the detrapping rate D . A comparable activation energy can be extracted from the temperature evolution of τ_l measured on the HPHT-15° sample. We deduce that the exciton trapping potential at the interface is of the order of 100 meV for these samples whose twist angle is of the order of 10-15°. This experimental measurement of a shallow trapping of exciton at the twisted interface is in agreement with previous theoretical calculation [41, 42],

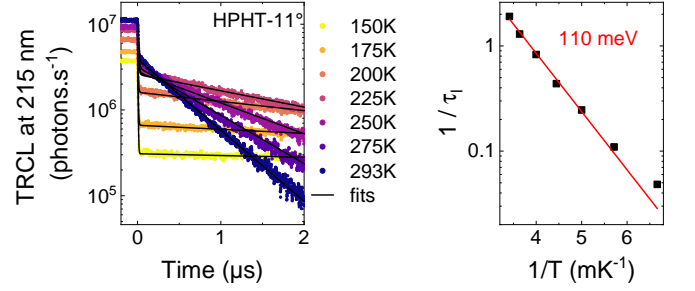


FIGURE 8. (a) TRCL decays of free exciton luminescence for temperatures in the range 150 - 293K on HPHT-11° sample. Bi-exponential decays are used in the fits to extract the characteristic time of the long component τ_l . (b) $1/\tau_l$ as a function of $1/T$ in the HPHT-11° sample. An Arrhenius law is fitted from which a 110 meV activation energy is deduced.

and evidence that the 2 eV redshift of the interface luminescence does not come from a giant Moiré trapping, as suggested by previous studies [39, 40].

In summary, we propose a scenario of excitons accumulating at the interface in a non-radiative excitons X_{2D} form and their subsequent self-trapping. This phenomenological description accounts for the observed luminescence decay and is consistent with the luminescence efficiencies close to 100% measured for 30° twist at 300 K for the recombination of self-trapped excitons. It was also concluded that for intermediate twist angles, on the HPHT-11° and HPHT-15° samples, the long decay time between 150 and 300 K is limited by the rate of exciton detrapping from the interface. Thermal activation of detrapping revealed an interface exciton trapping potential of the order of 100 meV for both samples, in agreement with theoretical estimates [41, 42].

VII - Discussion : Self-trapping in sp^2 BN

We now discuss the origin of the exciton self-trapping in hBN. First, exciton self-trapping is favored by the ability of the lattice to deform around the exciton, and second, it is facilitated by the ability of the exciton to be localized in the deformed area it has induced. Given the high ionicity of hBN, exciton formation involves the transfer of charge from a boron atom (hole on boron) to a nitrogen atom (electron on nitrogen), as illustrated by theoretical calculations of the intensity of the exciton wave function [77, 78]. This charge transfer induces the formation of a dipole to which the ionic lattice is sensitive. Furthermore, due to the high compactness of the hBN exciton [50], the size of the dipole it forms is comparable to that of dipoles formed by ionic bonds, so the lattice-exciton interaction is relatively strong in hBN. These features are highly beneficial for exciton self-trapping in hBN, yet the latter is not observed in the defect-free crystal. In our study, it appears only after

their localization at a highly disoriented interface. On the one hand, at low twist angles, a Moiré superlattice and a resulting periodic superpotential appears and may interact with excitons [18–24]. On the other hand, at a high degree of twist, a transition from a commensurable to an incommensurable lattice occurs, as studied in quasicrystals, leading to a drastic change in the structure and the physical phenomena it can host. While at low hBN-hBN twist angles, the perturbation of the charge distribution induced by the appearance of the π^{B-B} and π^{N-N} homo-bonds is weak and confined to certain zones of the Moiré structure; at high angles a very large fraction of the π -bonds are perturbed and densely distributed all over the interface. As a result, the potential perturbations increase in locality and density with increasing twist angle, which locally boost the ionic character of the lattice, and as a consequence, the exciton-lattice interaction. In addition, the lattice deformability is likely to be locally strongest at high angles. These two elements address the role of the twist angle on exciton self-trapping, but also highlight the need for further theoretical studies to better understand the origin of exciton self-trapping at the twisted interface, by exploring which atomic sites host self-trapped excitons and which lattice distortion are involved.

The luminescence signal at 300 nm from self-trapped excitons at the interface is likely to be related to a similar signal previously observed in some defected hBN samples [79] as well as in other sp^2 -hybridized BN samples that exhibit interface disorder, such as turbostratic BN, pyrolytic BN, or BN multiwall nanotubes [80, 81]. Also broad, centered around 4 eV and with long decay dynamics, this emission appears only above 6 eV excitation, i.e. above the excitonic bandgap, suggesting its excitonic origin and a 2 eV energy shift. This emission could also be related to exciton self-trapping, which would then appear to be a fairly common phenomenon in these materials, in the native stacking defect of hBN and more generally in sp^2 BN.

Recent studies report unusual exciton-lattice interactions at other h2D interfaces [82–85], which in some cases could lead to the formation of self-trapped excitons [85]. Our results added to these studies show that the properties of these self-trapped states are easily modulated by the structural properties of h2Ds, such as the twist angle, the choice of stacking, or the thickness of the crystals. h2Ds appear to be an ideal platform for studying and manipulating self-trapped states, opening up new fields of application for these materials. In particular, the high efficiency and the large broadening of the 300 nm luminescence of self-trapped excitons at twisted hBN-hBN interfaces could be exploited for broadband UV light sources [86–89]. Finally, the formation of interlayer excitons at the interfaces between two TMDs, (with hole and electron spatially separated in the two layers), has been shown to increase the exciton lifetime by more than 3

orders of magnitude [7–10]. The long lifetime and dark character of the X_{2D} excitons at the hBN-hBN interface might point towards interlayer excitons.

VIII - Conclusion

Sixteen twisted hBN-hBN homostructures have been studied using CL and TRCL as function of temperature with the aim of understanding the broad luminescence observed at a wavelength around 300 nm in hBN-hBN homostructures. Our study shows that this luminescence is indirectly excited by the transport of free excitons from the volume of the flakes to the interface via their diffusion. We have shown that the internal quantum yield of the luminescence at 300 nm is close to 100% at angles close to 30° on HPHT samples. This luminescence is attributed to the radiative recombination of self-trapped excitons at the interface. The exciton dipole induces a local deformation of the interface lattice, in which the exciton is "self-trapped".

TRCL luminescence decays could be analyzed by considering a trapping-detrapping model where 3 exciton populations are coupled : a population of free excitons in the volume (X_{3D}), a population of excitons trapped at the 2D interface (X_{2D} , not self-trapped), and a population of excitons self-trapped at the interface (X_{ST}). In this scenario, which is consistent with our experimental data set, excitons accumulate at the interface in a non-radiative (dark) and long living X_{2D} form. Analysis of the data as a function of temperature revealed a self-trapping energy barrier of the order of 10 meV and an interface trapping potential for excitons of about 100 meV on two samples with twist angles of 11 and 15°. These values agree with the literature and theoretical calculations available to date.

For highly twisted hBN-hBN structures, the ionic character and the deformability of the lattice are locally and densely perturbed across the entire interface, which is probably at the root of exciton self-trapping. Beyond these qualitative elements, it remains to be understood in detail what is the key element that causes self-trapping only at high angles, and further theoretical studies would be welcome. Moreover, the physical phenomena occurring in h2Ds at high angles are very different from those at small angles with Moiré superstructures. To explore them, one avenue would be to apply the quasi-crystal physics to h2Ds with high twist angles.

Acknowledgments

The research leading to these results has received funding European Union's Horizon 2020 research and innovation program under grant agreements No 785219 (Graphene Core 2) and No 881603 (Graphene Core 3). Sup-

port for the APHT hBN crystal growth comes from the Office of Naval Research, Award No. N00014-20-1-2474. K.W. and T.T. acknowledge support from the JSPS KAKENHI (Grant Numbers 21H05233 and 23H02052) and World Premier International Research Center Initiative (WPI), MEXT, Japan. This work was also supported by Agence Nationale de la Recherche funding under the program ESR/EquipEx+ (grant number ANR-21-ESRE-0025) and ANR ATOEMS.

Appendices

Appendix A : Measurement of the internal quantum efficiency of the broad 300 nm luminescence.

The procedure to measure the internal quantum efficiency (*IQE*) of a luminescence band during cw-CL experiment is described in ref. [51]. In this reference, it is applied to measure the *IQE* of the free exciton luminescence of hBN single crystals that appears at 215 nm. To apply the same procedure to the 300 nm band, one should consider the significative change of the refractive index of the top surface between 215 and 300 nm.

In our case, the CL intensity is integrated between 240 and 400 nm as shown in Fig. 9. The reflection index n of the surface decreases from $n=3$ to $n=2.37$ over the 240-400 nm range [?], corresponding to a light extraction that varies from 2.1% to 3.9%. To simply measure the magnitude of the *IQE* of this band, we approximate a constant index $n=2.56$ measured at the band maximum (3.2% extraction). This approximation is reasonable given the uncertainty of the *IQE* measurement, which is of the order of 50% [51].

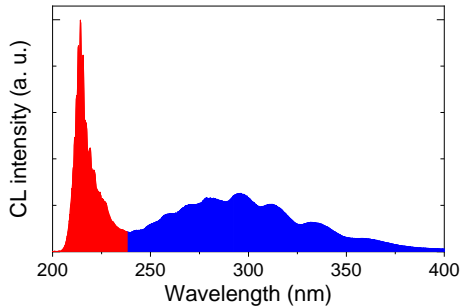


FIGURE 9. Corrected CL spectrum of a hBN-hBN homostructure at 300 K. The integrated intensity of the free exciton band of hBN appears in red, and the integrated intensity of the broad optical emission at 300 nm, characteristic of twisted hBN-hBN homostructures, appears in blue.

Appendix B : Measurement of the twist angle by electron diffraction.

The twist angle of hBN-hBN homostructure was determined by Electron Backscatter Diffraction (EBSD) and Electron Channeling Pattern (ECP).

In EBSD, the surface crystal orientations of a sample in the SEM are determined for each diffraction pattern using the OIM Analysis software from EDAX. For hBN-hBN homostructures, the crystal orientation of the top crystal is expressed in the reference frame of the bottom crystal. Not surprisingly, the out-of-plane z-axis of the two hBN crystals is identical. On the other hand, different in-plane orientations are measured as shown in Fig. 1(b) in the main text. The twist angle between the two crystals corresponds to this difference in orientation. It is equivalent to the smallest angle that can be found between the atomic B-N bonds of the two crystal lattices, regardless of their orientation (B to N or N to B). Between two hBN crystals this angle varies between 0 and 30°. EBSD mapping can quickly measure the orientation of several crystals separated by a few millimeters with an accuracy of the order of 1° (Fig. 1(b)).

In ECP, mapping is not possible, but the diffraction pattern on a selected zone of a 2D crystal gives its in-plane crystal orientation directly, without the need for complex processing. By comparing the ECP images of two 2D crystals placed on top of each other, we can measure the twist angle between the two crystals with an accuracy of the order of 1°. Its absolute value varies between 0 and 30° and corresponds to the angle measured by EBSD, as shown in Fig. 1(c).

Appendix C : CL signal on low angle hBN-hBN structures.

Fig. 10 shows spectra measured on a slightly twisted PDC sample in green and a highly twisted PDC sample in red, compared to a spectrum measured on a single PDC crystal in black. The single crystal shows emission from point defects (labeled α , β , γ) that occur locally in some crystals. As shown in Fig. 4(c) of the main text, the CL intensity of the hBN-hBN interface decreases with decreasing twist angle. For the PDC-2° sample, the intensity of the interface luminescence is lower than the intensity of the native color center emission. To avoid confusion between native defects and interface emission, only highly twisted single crystal structures without significant native defect emission in the 200-400 nm range have been investigated.

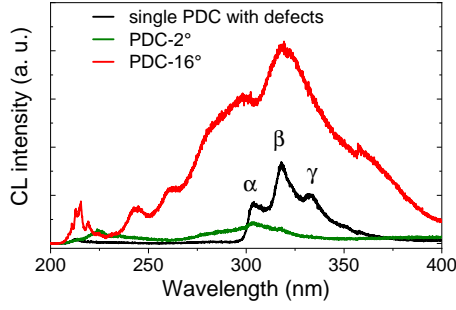


FIGURE 10. CL spectra measured at 300 K on PDC-2°, PDC-16°, and on a single PDC crystal under the same excitation conditions (3 kV, 280 pA).

Appendix D : Luminescence decay as function of the energy within the broad 300 nm luminescence.

Given the linewidth of the emission at 300 nm, which extends between 250 and 400 nm (i.e., nearly 2 eV), the question arises whether it is the result of a population of emitters of different energies or whether the signal is intrinsically broad. To check this, the decay of the luminescence is studied at different energies of the broad emission.

Fig. 11(a) shows the spectrum of the APHT-28° sample, dominated by the luminescence of interest with little Fabry-Pérot interference contrast. Fig. 11(b) shows the TRCL decays of the filtered luminescence at different wavelengths (± 7.5 nm). The decay dynamics are perfectly identical for all investigated wavelengths. This result suggests a unique recombination mechanism for this particularly broad band. The large spectral width of the 300 nm band thus appears to be an intrinsic feature of the luminescence process of twisted hBN-hBN homostructures.

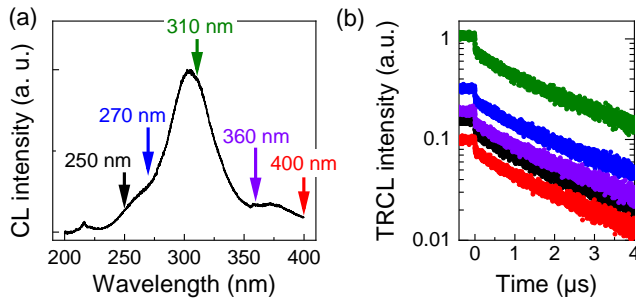


FIGURE 11. CL spectrum (3 kV, 280 pA) measured on the APHT-28° homostructure at 300 K. (b) Decay of the luminescence intensity, filtered at different wavelengths, recorded in TRCL after the excitation was stopped at $t = 0$. The wavelengths corresponding to each color are indicated by arrows in (a).

Appendix E : Low temperature spectrum of twisted hBN-hBN homostructure.

Fig. 12 shows spectra obtained on a 23° twisted hBN-hBN structure and on a hBN single crystal at room temperature and at cryogenic temperature. On the single crystal, the luminescence is dominated by the free exciton luminescence occurring at 215 nm, while on the hBN-hBN structure the emission is dominated by the broad luminescence occurring between 250 and 400 nm. The band is modulated by Fabry-Perot interference. We observe that the band remains extremely broad even at cryogenic temperatures. A color center emission also appears on the hBN-hBN structure and on the single hBN crystals, with a zero-phonon band at 305 nm (α) and its phonon replica (β and γ). This emission shows a large thermal broadening typical of color centers, indicating that its nature is different from that of the hBN-hBN interface emission, whose broadening remains around 2 eV even when the sample holder temperature reaches 5 K.

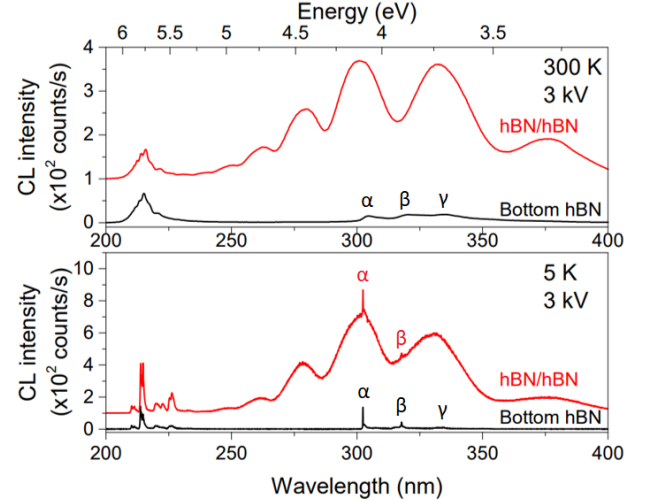


FIGURE 12. CL spectra measured at room and cryogenic temperature on a single hBN flake, in black, and on a hBN-hBN homostructure with a 23° twist, in red, both fabricated from the same HPHT crystal.

Appendix F : Simulation of TRCL decays with rate equations.

The TRCL decay of the luminescence intensity is related to the evolution of the exciton populations and thus to their interactions. The scenario of exciton population interactions discussed in the main text is the following : the free exciton population N_{X3D} , generated in the crystal volume by the primary excitation, are trapped (rate C) at the interface. The excitons accumulate at the 2D interface under a dark and long living form (N_{X2D} population). They are finally converted into N_{XST} by their

self-trapping (rate ST) and into N_{X3D} by their detrapping (rate D). This scenario, illustrated in Fig. 7 of the main text, leads to the following differential equations :

$$\begin{cases} \frac{dN_{X3D}}{dt} = -\frac{N_{X3D}}{\tau_0} - N_{X3D} \times C + N_{X2D} \times D + G(t) \\ \frac{dN_{X2D}}{dt} = -N_{X2D}(D + ST) + N_{X3D} \times C \\ \frac{dN_{XST}}{dt} = -\frac{N_{XST}}{\tau_{XST}} + N_{X2D} \times ST \end{cases} \quad (1)$$

where τ_0 is the lifetime of the free exciton in the volume (without interface) and τ_{XST} is the lifetime of the X_{ST} excitons. G denotes the generation rate of free excitons, which is constant during continuous excitation and then zero when the excitation stops. A priori, C varies slightly with temperature due to the weak evolution of the exciton diffusion length with temperature [61], while the rates of D and ST are thermally activated.

The first two equations of the system are not coupled to N_{XST} , they could be considered independently. We find a superposition of two exponential decays for both N_{X3D} and N_{X2D} exciton populations : one short with a characteristic time τ_s and the other long with a characteristic time $\tau_l > \tau_s$. These times can be written with $A = 1/\tau_0 + C$, and $B = D + ST$:

$$\frac{1}{\tau_s} = \frac{A + B + \sqrt{(A - B)^2 + 4CD}}{2} \quad (2)$$

$$\frac{1}{\tau_l} = \frac{A + B - \sqrt{(A - B)^2 + 4CD}}{2} \quad (3)$$

The interruption of the steady excitation at the initial time results in $G(t) = 0$ for $t > 0$. The previously established steady equilibrium imposes the initial conditions :

$$\frac{N_{X2D}(0)}{N_{X3D}(0)} = \frac{C}{B} \quad (4)$$

And the N_{X3D} population is written as :

$$\frac{N_{X3D}(t)}{N_{X3D}(0)} = A_l e^{-\frac{t}{\tau_l}} + (1 - A_l) e^{-\frac{t}{\tau_s}} \quad (5)$$

With the weight of the long exponential, A_l , given by :

$$A_l = \frac{\tau_l}{\tau_l - \tau_s} \left(1 - \frac{1}{B\tau_l} \right) \approx 1 - \frac{1}{B\tau_l} \quad (6)$$

This gives :

$$B = \frac{1}{\tau_l} \frac{1}{1 - A_l} \quad (7)$$

The parameter $B = D + ST$ can therefore be extracted from the TRCL decays of the free exciton luminescence

from the previous equation, or from the simplified form when $A_l \ll 1$:

$$D + ST \approx \frac{1}{\tau_l} \quad (8)$$

Calculations show that all three populations follow the same decay time, as can be seen in Fig. 13(a), which is consistent with the experimentally observed decays of the N_{XST} and N_{X3D} populations in Fig. 13(a) (see also Fig. 3(b) in the main text). The long component of the TRCL decay being governed by the detrapping and self-trapping rates of the N_{X2D} population that occurs in the long term.

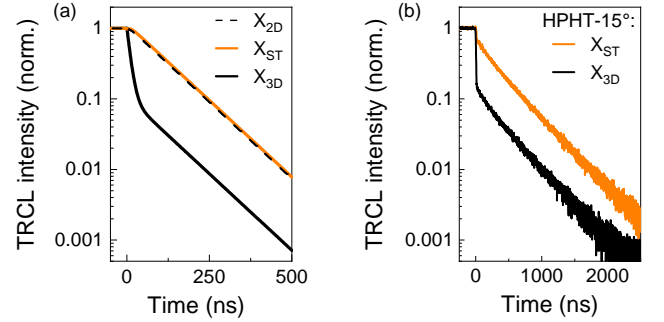


FIGURE 13. (a) Theoretical decays of the N_{X2D} and N_{X3D} exciton populations for $\tau_s=10$ ns, $\tau_l=100$ ns and $A_l=0.1$, and of the N_{XST} self-trapped exciton population for $\tau_{XST} = 10$ ns. (b) Experimental decays for the N_{XST} (at 300 nm) and N_{X3D} (at 215 nm) exciton populations on the HPHT-15° structure measured in TRCL at 5 kV, 27 pA, 300 K.

* sroux@insa-toulouse.fr

- [1] A. K. Geim and I. V. Grigorieva, Van der waals heterostructures, *Nature* **499**, 419 (2013).
- [2] J. F. Sierra, J. Fabian, R. K. Kawakami, S. Roche, and S. O. Valenzuela, Van der waals heterostructures for spintronics and opto-spintronics, *Nature Nanotechnology* **16**, 856 (2021).
- [3] C. N. Lau, M. W. Bockrath, K. F. Mak, and F. Zhang, Reproducibility in the fabrication and physics of moiré materials, *Nature* **602**, 41 (2022).
- [4] M. Gibertini, M. Koperski, A. F. Morpurgo, and K. S. Novoselov, Magnetic 2d materials and heterostructures, *Nature nanotechnology* **14**, 408 (2019).
- [5] H. Fang, B. Han, C. Robert, M. Semina, D. Lagarde, E. Courtade, T. Taniguchi, K. Watanabe, T. Amand, B. Urbaszek, *et al.*, Control of the exciton radiative lifetime in van der waals heterostructures, *Physical review letters* **123**, 067401 (2019).
- [6] J. Choi, M. Florian, A. Steinhoff, D. Erben, K. Tran, D. S. Kim, L. Sun, J. Quan, R. Claassen, S. Majumder, *et al.*, Twist angle-dependent interlayer exciton lifetimes in van der waals heterostructures, *Physical Review Letters* **126**, 047401 (2021).

- [7] P. Rivera, J. R. Schaibley, A. M. Jones, J. S. Ross, S. Wu, G. Aivazian, P. Klement, K. Seyler, G. Clark, N. J. Ghimire, *et al.*, Observation of long-lived interlayer excitons in monolayer mose2-wse2 heterostructures, *Nature communications* **6**, 6242 (2015).
- [8] S. Ovesen, S. Brem, C. Linderälv, M. Kuisma, T. Korn, P. Erhart, M. Selig, and E. Malic, Interlayer exciton dynamics in van der waals heterostructures, *Communications Physics* **2**, 23 (2019).
- [9] B. Miller, A. Steinhoff, B. Pano, J. Klein, F. Jahnke, A. Holleitner, and U. Wurstbauer, Long-lived direct and indirect interlayer excitons in van der waals heterostructures, *Nano letters* **17**, 5229 (2017).
- [10] L. Yuan, B. Zheng, J. Kunstmann, T. Brumme, A. B. Kuc, C. Ma, S. Deng, D. Blach, A. Pan, and L. Huang, Twist-angle-dependent interlayer exciton diffusion in ws2-wse2 heterobilayers, *Nature materials* **19**, 617 (2020).
- [11] F. Cadiz, E. Courtade, C. Robert, G. Wang, Y. Shen, H. Cai, T. Taniguchi, K. Watanabe, H. Carrere, D. Lagarde, *et al.*, Excitonic linewidth approaching the homogeneous limit in mos2 -based van der waals heterostructures, *Physical Review X* **7**, 021026 (2017).
- [12] P. Rivera, K. L. Seyler, H. Yu, J. R. Schaibley, J. Yan, D. G. Mandrus, W. Yao, and X. Xu, Valley-polarized exciton dynamics in a 2d semiconductor heterostructure, *Science* **351**, 688 (2016).
- [13] J. Kim, C. Jin, B. Chen, H. Cai, T. Zhao, P. Lee, S. Kahn, K. Watanabe, T. Taniguchi, S. Tongay, *et al.*, Observation of ultralong valley lifetime in wse2/mos2 heterostructures, *Science advances* **3**, e1700518 (2017).
- [14] E. Carré, *Propriétés optiques du phosphore noir : du cristal massif aux couches atomiques*, Ph.D. thesis (2022).
- [15] S. Latini, T. Olsen, and K. S. Thygesen, Excitons in van der waals heterostructures : The important role of dielectric screening, *Physical Review B* **92**, 245123 (2015).
- [16] Y. Lin, X. Ling, L. Yu, S. Huang, A. L. Hsu, Y.-H. Lee, J. Kong, M. S. Dresselhaus, and T. Palacios, Dielectric screening of excitons and trions in single-layer mos2 , *Nano letters* **14**, 5569 (2014).
- [17] W.-T. Hsu, J. Quan, C.-Y. Wang, L.-S. Lu, M. Campbell, W.-H. Chang, L.-J. Li, X. Li, and C.-K. Shih, Dielectric impact on exciton binding energy and quasiparticle band-gap in monolayer ws2 and wse2 , *2D Materials* **6**, 025028 (2019).
- [18] E. M. Alexeev, D. A. Ruiz-Tijerina, M. Danovich, M. J. Hamer, D. J. Terry, P. K. Nayak, S. Ahn, S. Pak, J. Lee, J. I. Sohn, *et al.*, Resonantly hybridized excitons in moiré superlattices in van der waals heterostructures, *Nature* **567**, 81 (2019).
- [19] C. Jin, E. C. Regan, A. Yan, M. Iqbal Bakti Utama, D. Wang, S. Zhao, Y. Qin, S. Yang, Z. Zheng, S. Shi, *et al.*, Observation of moiré excitons in wse2/ws2 heterostructure superlattices, *Nature* **567**, 76 (2019).
- [20] K. L. Seyler, P. Rivera, H. Yu, N. P. Wilson, E. L. Ray, D. G. Mandrus, J. Yan, W. Yao, and X. Xu, Signatures of moiré-trapped valley excitons in mose2/wse2 heterobilayers, *Nature* **567**, 66 (2019).
- [21] K. Tran, G. Moody, F. Wu, X. Lu, J. Choi, K. Kim, A. Rai, D. A. Sanchez, J. Quan, A. Singh, *et al.*, Evidence for moiré excitons in van der waals heterostructures, *Nature* **567**, 71 (2019).
- [22] H. Baek, M. Brotons-Gisbert, Z. X. Koong, A. Campbell, M. Rambach, K. Watanabe, T. Taniguchi, and B. D. Gerardot, Highly energy-tunable quantum light from moiré-trapped excitons, *Science advances* **6**, eaba8526 (2020).
- [23] S. Brem, C. Linderälv, P. Erhart, and E. Malic, Tunable phases of moiré excitons in van der waals heterostructures, *Nano letters* **20**, 8534 (2020).
- [24] M. Brotons-Gisbert, H. Baek, A. Molina-Sánchez, A. Campbell, E. Scerri, D. White, K. Watanabe, T. Taniguchi, C. Bonato, and B. D. Gerardot, Spin-layer locking of interlayer excitons trapped in moiré potentials, *Nature Materials* **19**, 630 (2020).
- [25] D. Unuchek, A. Ciarrocchi, A. Avsar, K. Watanabe, T. Taniguchi, and A. Kis, Room-temperature electrical control of exciton flux in a van der waals heterostructure, *Nature* **560**, 340 (2018).
- [26] D. Unuchek, A. Ciarrocchi, A. Avsar, Z. Sun, K. Watanabe, T. Taniguchi, and A. Kis, Valley-polarized exciton currents in a van der waals heterostructure, *Nature nanotechnology* **14**, 1104 (2019).
- [27] C. Gong and X. Zhang, Two-dimensional magnetic crystals and emergent heterostructure devices, *Science* **363**, eaav4450 (2019).
- [28] Y. Wang, Y. Shao, D. W. Matson, J. Li, and Y. Lin, Nitrogen-doped graphene and its application in electrochemical biosensing, *ACS nano* **4**, 1790 (2010).
- [29] C. R. Dean, A. F. Young, I. Meric, C. Lee, L. Wang, S. Sorgenfrei, K. Watanabe, T. Taniguchi, P. Kim, K. L. Shepard, *et al.*, Boron nitride substrates for high-quality graphene electronics, *Nature nanotechnology* **5**, 722 (2010).
- [30] H. Arora, Y. Jung, T. Venanzi, K. Watanabe, T. Taniguchi, R. Hubner, H. Schneider, M. Helm, J. C. Hone, and A. Erbe, Effective hexagonal boron nitride passivation of few-layered inorganic and organic electronic and optical properties, *ACS applied materials & interfaces* **11**, 43480 (2019).
- [31] B. Huang, G. Clark, D. R. Klein, D. MacNeill, E. Navarro-Moratalla, K. L. Seyler, N. Wilson, M. A. McGuire, D. H. Cobden, D. Xiao, *et al.*, Electrical control of 2d magnetism in bilayer crI3 , *Nature nanotechnology* **13**, 544 (2018).
- [32] H. H. Kim, B. Yang, S. Li, S. Jiang, C. Jin, Z. Tao, G. Nichols, F. Sfigakis, S. Zhong, C. Li, *et al.*, Evolution of interlayer and intralayer magnetism in three atomically thin chromium trihalides, *Proceedings of the National Academy of Sciences* **116**, 11131 (2019).
- [33] K. Yasuda, X. Wang, K. Watanabe, T. Taniguchi, and P. Jarillo-Herrero, Stacking-engineered ferroelectricity in bilayer boron nitride, *Science* **372**, 1458 (2021).
- [34] C. Woods, P. Ares, H. Nevison-Andrews, M. Holwill, R. Fabregas, F. Guinea, A. Geim, K. Novoselov, N. Wale, and L. Fumagalli, Charge-polarized interfacial superlattices in marginally twisted hexagonal boron nitride, *Nature communications* **12**, 347 (2021).
- [35] X.-J. Zhao, Y. Yang, D.-B. Zhang, and S.-H. Wei, Formation of bloch flat bands in polar twisted bilayers without magic angles, *Physical review letters* **124**, 086401 (2020).
- [36] X.-J. Zhao, Y. Yang, D.-B. Zhang, and S.-H. Wei, Flat bands in twisted bilayers of polar two-dimensional semiconductors, *Physical Review Materials* **5**, 014007 (2021).
- [37] K. Yao, N. R. Finney, J. Zhang, S. L. Moore, L. Xian, N. Tancogne-Dejean, F. Liu, J. Ardelean, X. Xu, D. O. Halbertal, K. Watanabe, T. Taniguchi, H. Ochoa, A. Asenjo-Garcia, X. Zhu, D. N. Basov, A. Rubio, C. R. Dean, J. Hone, and P. J. Schuck, Enhanced tunable se-

- cond harmonic generation from twistable interfaces and vertical superlattices in boron nitride homostructures, *Science Advances* **7**, eabe8691 (2021).
- [38] A. Plaud, *Excitons dans le nitrure de bore lamellaire : étude des phases hexagonale, rhomboédrique et d'hétérostructures 2D*, Ph.D. thesis (2020).
- [39] H. J. Lee, M. M. Al Ezzi, N. Raghuvanshi, J. Y. Chung, K. Watanabe, T. Taniguchi, S. Garaj, S. Adam, and S. Gradecak, Tunable optical properties of thin films controlled by the interface twist angle, *Nano Letters* **21**, 2832 (2021).
- [40] Y. Li, X. Xie, H. Zeng, B. Li, Z. Zhang, S. Wang, J. Liu, and D. Shen, Giant moiré trapping of excitons in twisted hbn, *Optics Express* **30**, 10596 (2022).
- [41] C. Su, F. Zhang, S. Kahn, B. Shevitski, J. Jiang, C. Dai, A. Ungar, J.-H. Park, K. Watanabe, T. Taniguchi, J. Kong, Z. Tang, W. Zhang, F. Wang, M. Crommie, S. G. Louie, S. Aloni, and A. Zettl, Tuning colour centres at a twisted hexagonal boron nitride interface, *Nature Materials* **21**, 896 (2022).
- [42] S. Latil, H. Amara, and L. Sponza, Structural classification of boron nitride twisted bilayers and ab initio investigation of their stacking-dependent electronic structure, *SciPost Physics* (2023).
- [43] L. D. Landau, The movement of electrons in the crystal lattice, *Physikalische Zeitschrift der Sowjetunion* **3**, 644 (1933).
- [44] J. Frenkel, On the solid body model of heavy nuclei, *Physikalische Zeitschrift der Sowjetunion* **9** (1936).
- [45] T. G. Castner and W. Känzig, The electronic structure of v-centers, *Journal of Physics and Chemistry of Solids* **3**, 178 (1957).
- [46] M. N. Kabler, Low-temperature recombination luminescence in alkali halide crystals, *Physical Review* **136** (1964).
- [47] R. B. Murray and F. J. Keller, Recombination luminescence from v_K centers in potassium iodide, *Physical Review* **137** (1965).
- [48] J. Ramamurti and K. Teegarden, Intrinsic luminescence of rbi and ki at 10k, *Physical Review* **145** (1966).
- [49] R. A. Kink, G. G. Liidja, C. B. Lushchik, and T. A. Soovik, Bulletin of the russian academy of sciences : Physics, **31** **2030** (1967).
- [50] S. Roux, C. Arnold, F. Paleari, L. Sponza, E. Janzen, J. Edgar, B. Toury, C. Journet, V. Garnier, P. Steyer, T. Taniguchi, K. Watanabe, F. Ducastelle, A. Loiseau, and J. Barjon, Radiative lifetime of free excitons in hexagonal boron nitride, *Physical Review B* **104**, L161203 (2021).
- [51] L. Schué, L. Sponza, A. Plaud, H. Bensalah, K. Watanabe, T. Taniguchi, F. Ducastelle, A. Loiseau, and J. Barjon, Bright luminescence from indirect and strongly bound excitons in h-bn, *Physical review letters* **122**, 067401 (2019).
- [52] S. Liu, R. He, L. Xue, J. Li, B. Liu, and J. H. Edgar, Single crystal growth of millimeter-sized monoisotopic hexagonal boron nitride, *Chemistry of materials* **30**, 6222 (2018).
- [53] J. Li, C. Elias, G. Ye, D. Evans, S. Liu, R. He, G. Casabois, B. Gil, P. Valvin, B. Liu, *et al.*, Single crystal growth of monoisotopic hexagonal boron nitride from a fe-cr flux, *Journal of Materials Chemistry C* **8**, 9931 (2020).
- [54] Y. Kubota, K. Watanabe, O. Tsuda, and T. Taniguchi, Deep ultraviolet light-emitting hexagonal boron nitride synthesized at atmospheric pressure, *Science* **317**, 932 (2007).
- [55] K. Watanabe, T. Taniguchi, and H. Kanda, Direct-bandgap properties and evidence for ultraviolet lasing of hexagonal boron nitride single crystal, *Nature materials* **3**, 404 (2004).
- [56] T. Taniguchi and K. Watanabe, Synthesis of high-purity boron nitride single crystals under high pressure by using ba-bn solvent, *Journal of crystal growth* **303**, 525 (2007).
- [57] Y. Li, V. Garnier, P. Steyer, C. Journet, and B. Toury, Millimeter-scale hexagonal boron nitride single crystals for nanosheet generation, *ACS Applied Nano Materials* **3**, 1508 (2020).
- [58] Y. Li, V. Garnier, C. Journet, J. Barjon, A. Loiseau, I. Stenger, A. Plaud, B. Toury, and P. Steyer, Advanced synthesis of highly crystallized hexagonal boron nitride by coupling polymer-derived ceramics and spark plasma sintering processes—influence of the crystallization promoter and sintering temperature, *Nanotechnology* **30**, 035604 (2018).
- [59] A. Castellanos-Gomez, M. Buscema, R. Molenaar, V. Singh, L. Janssen, H. S. J. van der Zant, and G. A. Steele, Deterministic transfer of two-dimensional materials by all-dry viscoelastic stamping, *2D Materials* **1** (2014).
- [60] K. S. Novoselov, A. K. Geim, S. V. Morozov, D. Jiang, Y. Zhang, S. V. Dubonos, I. V. Grigorieva, and A. A. Firsov, Electric field effect in atomically thin carbon films, *Science* **306** (2004).
- [61] S. Roux, C. Arnold, E. Carré, E. Janzen, J. H. Edgar, C. Maestre, B. Toury, C. Journet, V. Garnier, P. Steyer, *et al.*, Surface recombination and out of plane diffusivity of free excitons in hexagonal boron nitride, *arXiv preprint arXiv :2308.05539* (2023).
- [62] Y. Peter and M. Cardona, *Fundamentals of semiconductors : physics and materials properties* (Springer Science & Business Media, 2010).
- [63] J. I. Pankove, *Optical processes in semiconductors* (Courier Corporation, 1975).
- [64] Y. Toyozawa, Theory of line-shapes of the exciton absorption bands, *Progress of Theoretical Physics* **20**, 53 (1958).
- [65] E. I. Rashba, Theory of strong interactions of electron excitations with lattice vibrations in molecular crystals, *Optika I Spektroskopiya* **2** (1957).
- [66] E. I. Rashba, Self-trapping of excitons, *Excitons*, edited by E. I. Rasha and M. D. Sturge (1982).
- [67] H. Sumi and T. Y., Urbach-martienssen rule and exciton trapped momentarily by lattice vibration, *Journal of the Physical Society of Japan* **31** (1971).
- [68] H. Blume, M. P. Fontana, and W. J. van Sciver, Properties of exciton states in nai. ii. excitonic energy transfer to q and tl centers, *Physica status solidi* **31**, 133 (1969).
- [69] R. A. Kink and G. G. Liidja, *Soviet Physics, Solid State* **11** (1969).
- [70] C. Lushchik, Survey of luminescence in alkali halide crystals : (the period 1966–1969), *Journal of Luminescence* **1-2**, 594 (1970).
- [71] R. T. Williams and K. S. Song, The self-trapped exciton, *Journal of Physics and Chemistry of Solids* **51**, 679 (1990).
- [72] C. B. Lushchik, Free and self-trapped excitons in alkali halides : Spectra and dynamics, *Excitons*, edited by E. I.

- Rashba and M. D. Sturge (1982).
- [73] I. Y. Tekhver and V. V. Khizhnyakov, Transfer of electronic excitation during the course of vibrational relaxation, *Soviet Physics JETP* **19** (1974).
 - [74] T. Vuong, G. Cassaboïs, P. Valvin, A. Ouerghi, Y. Chasagneux, C. Voisin, and B. Gil, Phonon-photon mapping in a color center in hexagonal boron nitride, *Physical review letters* **117**, 097402 (2016).
 - [75] Y. K. Jung, S. Kim, Y. C. Kim, and A. Walsh, Low barrier for exciton self-trapping enables high photoluminescence quantum yield in $\text{Cs}_3\text{Cu}_2\text{I}_5$, *The Journal of Physical Chemistry Letters* **12**, 8447 (2021).
 - [76] A. Y. Kobitski, K. S. Zhuravlev, H. P. Wagner, and D. R. T. Zahn, Self-trapped exciton recombination in silicon nanocrystals, *Physical Review B* **63** (2001).
 - [77] F. Paleari, H. P. Miranda, A. Molina-Sánchez, and L. Wirtz, Exciton-phonon coupling in the ultraviolet absorption and emission spectra of bulk hexagonal boron nitride, *Physical review letters* **122**, 187401 (2019).
 - [78] F. Paleari, *First-principles approaches to the description of indirect absorption and luminescence spectroscopy : exciton-phonon coupling in hexagonal boron nitride*, Ph.D. thesis (2019).
 - [79] A. K. L. Museur, E. Feldbach, Defect-related photoluminescence of hexagonal boron nitride, *Physical Review B* **78** (2008).
 - [80] L. Museur and A. Kanaev, Photoluminescence properties of pyrolytic boron nitride, *Journal of Materials Science* **44**, 2560–2565 (2009).
 - [81] P. Jaffrennou, J. Barjon, T. Schmid, L. Museur, A. Kanaev, J.-S. Lauret, C. Y. Zhi, C. Tang, Y. Bando, D. Golberg, B. Attal-Tretout, F. Ducastelle, and A. Loiseau, Near-band-edge recombinations in multiwalled boron nitride nanotubes : Cathodoluminescence and photoluminescence spectroscopy measurements, *Physical Review B* **77** (2008).
 - [82] P. Merkl, C.-K. Yong, M. Liebich, I. Hofmeister, G. Berghäuser, E. Malic, and R. Huber, Proximity control of interlayer exciton-phonon hybridization in van der waals heterostructures, *Nature Communications* **12**, 1719 (2021).
 - [83] C. M. Chow, H. Yu, A. M. Jones, J. Yan, D. G. Mandrus, T. Taniguchi, K. Watanabe, W. Yao, and X. Xu, Unusual exciton-phonon interactions at van der waals engineered interfaces, *Nano letters* **17**, 1194 (2017).
 - [84] Z. Hennighausen, J. Moon, K. M. McCreary, C. H. Li, O. M. van't Erve, and B. T. Jonker, Interlayer exciton-phonon bound state in $\text{Bi}_2\text{Se}_3/\text{monolayer WS}_2$ van der waals heterostructures, *ACS nano* <https://doi.org/10.1021/acsnano.2c10313> (2023).
 - [85] J.-P. Deng, H.-J. Li, X.-F. Ma, X.-Y. Liu, Y. Cui, X.-J. Ma, Z.-Q. Li, and Z.-W. Wang, Self-trapped interlayer excitons in van der waals heterostructures, *The Journal of Physical Chemistry Letters* **13**, 3732 (2022).
 - [86] S. Wang, Y. Yao, J. Kong, S. Zhao, Z. Sun, Z. Wu, L. Li, and J. Luo, Highly efficient white-light emission in a polar two-dimensional hybrid perovskite, *Chemical Communications* **54**, 4053 (2018).
 - [87] T. Jun, T. Handa, K. Sim, S. Iimura, M. Sasase, J. Kim, Y. Kanemitsu, and H. Hosono, One-step solution synthesis of white-light-emitting films via dimensionality control of the Cs-Cu-I system, *APL Materials* **7**, 111113 (2019).
 - [88] X. Li, W. Li, M. Xia, C. Liu, N. Li, Z. Shi, Y. Xu, and X. Zhang, Facile melting-crystallization synthesis of $\text{Cs}_2\text{Na}_x\text{Ag}_{1-x}\text{InCl}_6$: Bi double perovskites for white light-emitting diodes, *Inorganic Chemistry* **61**, 5040 (2022).
 - [89] L. Lian, P. Zhang, G. Liang, S. Wang, X. Wang, Y. Wang, X. Zhang, J. Gao, D. Zhang, L. Gao, *et al.*, Efficient dual-band white-light emission with high color rendering from zero-dimensional organic copper iodide, *ACS applied materials & interfaces* **13**, 22749 (2021).